Hindawi
Shock and Vibration
Volume 2020, Article ID 7834765, 11 pages
https://doi.org/10.1155/2020/7834765

*Research Article*

# Impact Resistance Behavior of Reinforced Concrete Beams Deteriorated due to Repeated Freezing and Thawing

**Yusuke Kurihashi**,[1] **Yoshinori Nonomura**,[2] **and Hisashi Konno**[3]

[1]*Department of Geosciences and Civil Engineering, Kanazawa University, Kanazawa, Japan*
[2]*Materials Research Team, Civil Engineering Research Institute for Cold Region, PWRI, Hokkaido, Japan*
[3]*Structures Research Team, Civil Engineering Research Institute for Cold Region, PWRI, Hokkaido, Japan*

Correspondence should be addressed to Yusuke Kurihashi; kuri@se.kanazawa-u.ac.jp

Received 8 January 2020; Accepted 7 December 2020; Published 23 December 2020

Academic Editor: Fabio Rizzo



Many existing reinforced concrete (RC) structures constructed more than 50 years ago now require maintenance. This is especially true in cold, snowy regions where significant frost damage deterioration of RC structures becomes a severe problem. In this study, falling-weight impact tests were performed to investigate the impact resistance behavior of RC beams degraded by frost damage. An RC beam was subjected to approximately 900 freeze-thaw cycles to emulate the frost damage before the execution of the impact test. The surface of the beam was remarkably scaled, and its coarse aggregate was exposed. The degree of deterioration was evaluated by the distribution of ultrasonic propagation velocity. The following conclusions were drawn. (1) The ultrasonic propagation velocity of RC beams was significantly reduced following 872 freeze-thaw cycles. At the upper edge of the RC beam, the ultrasonic wave propagation velocity decreased from 4,000 m/s to 1,500 m/s in some parts. This corresponds to a relative dynamic elastic modulus of approximately 14%. (2) The residual deflection of RC beams with frost damage increased at most by 20% compared with beams without frost damage. The increase in residual deflection was primarily related to the peeling of concrete at the collision site and the opening of multiple bending cracks. (3) According to the existing residual deflection calculation formula, an increase of 20% in the residual deflection corresponds to a decrease of about 17% in the bending capacity of the RC beam. When the relationship between the degree of frost damage deterioration and the impact resistance of RC structures is defined, existing structures subjected to accidental impact force from rockfalls are safer and can be maintained more efficiently.

## 1. Introduction

Many existing reinforced concrete (RC) structures constructed more than 50 years ago require considerable maintenance. In particular, in cold, snowy regions, significant frost damage deterioration of RC structures has become a severe problem. Both the appearance and the structural performance of these structures have degraded (see Figure 1). Therefore, some research institutes have been promoting studies on the effects of frost damage on the material performance of concrete [1–7] and bond behavior with steel rebars [8–12]. Additionally, the load-carrying performance of RC members deteriorated by frost-damage has been examined [8, 13–20]. According to these studies, the relationship between the degree of frost damage deterioration of concrete and the load-bearing performance of RC structures has been identified. However, the number of the experimental studies that have been conducted on the impact-resistant behavior of RC structures has been limited.

In a previous study, the effects of frost damage degradation on the impact resistance of structures were investigated experimentally, such as wall railings and rockfall protection structures, subjected to collisions [21, 22]. As a result, it was clarified that the impact resistant capacity of the RC beam decreased, and the failure mode of RC beams likely shifted from bending to shearing owing to the frost damage of concrete (see Figure 2). However, these research results are for small RC beams with cross-sectional dimensions of

(a) (b)

Figure 1: Frost damage in existing structures. (a) Damaged reinforced concrete (RC) wall barrier on the highway. (b) Damaged condition of RC pier of a rock shed.

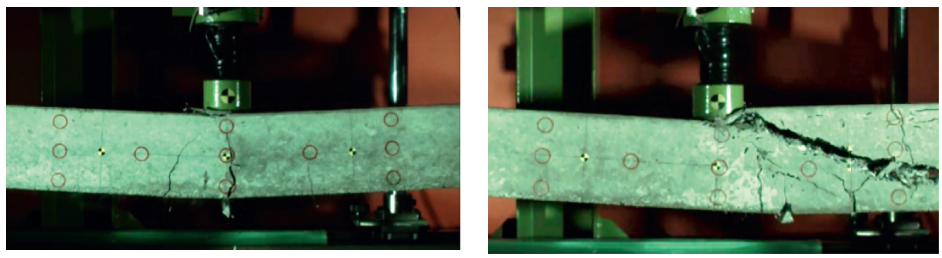

(a) (b)

Figure 2: Failure behavior of RC beam with/without frost damage after an impact loading test [22]. (a) Without frost damage. (b) With frost damage.

60 mm × 100 mm and no shear reinforcement. In contrast, structural members, such as the existing RC beams and columns, are usually provided with shear-reinforcing bars. They also have a broad cross section, so the fact that the degree of frost damage deterioration differs significantly between the surface and the inner parts of the member is considered. To evaluate the relationship between the degree of frost damage and structural performance, it is necessary to investigate RC members in conditions that resemble those of actual structures.

In this study, a drop-weight impact test of an RC beam having a cross-sectional dimension of 200 mm × 250 mm and a total length of 2 m was conducted to examine the impact resistance behavior of the RC beam that has been degraded by frost damage. Impact tests were performed after repeated freezing and thawing cycles that resulted in significant surface scaling and frost damage to the extent that the coarse aggregates were exposed. The degree of deterioration was evaluated based on an evaluation survey and the distribution of ultrasonic propagation velocity.

The determination of the relationship between the degree of frost damage deterioration and the impact resistance of the RC structures will enable safe and efficient maintenance of existing structures subjected to accidental impact force from rockfall.

## 2. Experimental Outline

*2.1. Overview of Specimens.* Table 1 shows the proportional mix of concrete used for the RC beams. In this study, the water/cement ratio (W/C) was set at 55% to promote freeze-thaw degradation. The minimum amount of admixture required for concrete casting was added to reduce the amount of air. To minimize the increase in strength from age during the test, early-strength cement was used, and the RC beams were cured for six weeks. Figure 3 shows the dimensions of the test specimen. The specimen used in this experiment was a double-reinforced rectangular RC beam with a cross-sectional dimension (width × height) of 200 mm × 250 mm. The net span length was set to 1.4 m because both ends of the beam significantly deteriorated, as described later in the study. Two D13 (SD345) bars were arranged on the top and bottom as axial reinforcement, and a D6 (SD295A) bar was used as shear reinforcement.

Table 1: Concrete composition and fresh properties.

| $W/C$ (%) | $S/(S+G)$ (%) | Unit mass (kg/m$^3$) | | | | Slump (cm) | Air (%) |
|---|---|---|---|---|---|---|---|
| | | $C$ | $W$ | $S$ | $G$ | | |
| 55 | 48 | 308 | 169 | 931 | 1,017 | 8.0 | 1.3 |

Table 2 shows a list of the calculated capacity of the beams. The flexural and shear load-carrying capacities in the table were calculated based on standard specifications of the Japanese Society of Civil Engineers (JCSE) [23]. The compressive strength of concrete without frost damage deterioration was 39.0 MPa. The yield strengths of the rebar were 353 MPa and 370 MPa at D13 and D6, respectively. The table shows that the calculated shear capacity divided by the calculated flexural capacity is 2.61, thus indicating that the design failure ultimately results from bending failure.

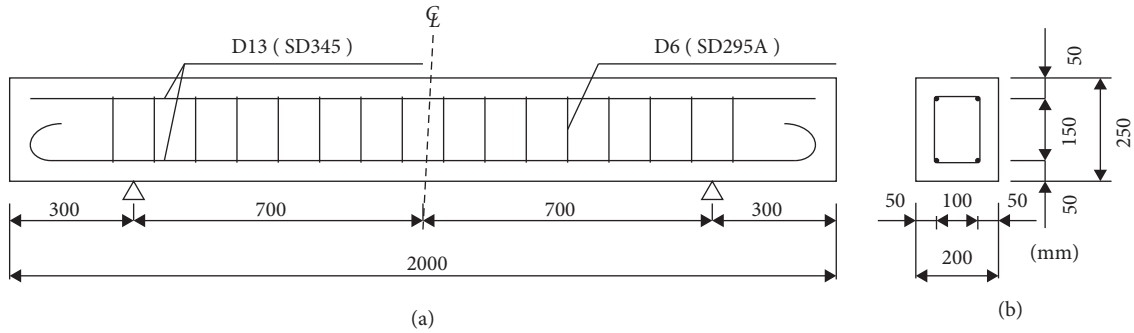


Figure 3: Outline of the test specimen. (a) Side view. (b) Sectional view.

Table 2: List of the calculated capacity of the beams.

| Flexural capacity $P_{uc}$ (kN) (1) | Shear capacity $V_{uc}$ (kN) | | | Shear-bending capacity (2)/(1) |
|---|---|---|---|---|
| | Concrete contribution | Rebar contribution | Total (2) | |
| 56.8 | 66.7 | 81.5 | 148 | 2.61 |

*2.2. Overview of Accelerated Deterioration owing to Successive Freeze-Thaw Cycles.* Accelerated deterioration owing to freezing and thawing was performed by aerial freezing and thawing in water based on JIS A 1148 [24]. As shown in Figure 4, the minimum and maximum temperatures of the concrete during the freeze-thaw cycle were −18°C and 5°C, respectively. The temperature was controlled by a sensor inserted in the center section of the beam span. The beam used for temperature control was not used for loading tests. The time required for one freeze-thaw cycle was approximately 7 h. A total of 872 cycles were executed. It is known that the concrete subjected to frost damage leads to decreased static elastic modulus and ultrasonic propagation velocity values [1, 25]. In this study, the ultrasonic propagation velocity in the beam width direction was measured by the transmission method at the positions shown in Figure 5 to evaluate the degree of frost damage deterioration of RC beams. The beam width was uniform and equal to 200 mm.

*2.3. Outline of Impact Loading Test.* Table 3 shows a list of test specimens. Specimens classified by N indicate no frost damage deterioration, whereas D indicates frost damage deterioration. $H$ defines the falling height of the weight (m). The height of the weight was set at two levels, namely, $H = 0.5$ and 1.0 m. In the case of D-H1.0, these items were then classified by serial numbers. In the impact loading experiment, a 300 kg steel weight with a tip diameter of 200 mm was dropped freely from the set falling height $H$ to the center of the span of the RC beam.

In this experiment, we adopted a single loading method wherein the free-fall test was performed once. Additionally, both fulcrums of the test specimen had a structure similar to a pin support that allowed for rotation and restrain lifting. The impact velocity of the weight was measured using a laser sensor. The impact loading test setup is shown in Figure 6.

The measurement items were the weight impact force and reaction force, impact velocity, and loading point deflection. The weight impact force (impact load) and the reaction force were measured with a strain–gauge load-cell type. The load point deflection was measured with a laser noncontact displacement meter. Cracking progress was recorded using a high-speed camera (progressive scan method, sensor resolution = 1024 × 1024 pixels). The frame rate was 2,000 frames per second.

## 3. Deterioration of Frost Damage of RC Beams

*3.1. Appearance.* Figure 7 shows the D-H0.5/H1.0 before the impact loading test as an example of the frost damage deterioration state. The photographs show that the concrete on the outer edge of the top surface of the beam exfoliated owing to frost damage, and coarse aggregate was exposed. In particular, the deterioration was remarkable at both ends of the beam because the frost damage deterioration gradually progressed by scaling of the surface of the beam.

*3.2. Water Absorption Ratio of Beam.* In this study, the 24 h water absorption of RC beam was measured, and the degree of frost damage on the beam was estimated. The measurement method is as follows. (1) First, the mass of the RC beam in the air-dried state was measured. (2) The RC beam was then placed in a water tank filled with tap water and soaked for 24 h. (3) Finally, the beam was lifted from the water tank, and the water on the surface was gently wiped off. The mass was measured again. The water absorption ratio $R_a$ was evaluated based on the following equation:

$$R_a = \frac{(W_w - W_d)}{W_d} \times 100, \quad (1)$$

where $W_w$ and $W_d$ are wet and dry masses of the beam.

Figure 8 shows the dry and wet masses and water absorption of each RC beam. From this figure, it is observed that the dry masses of N-beams are approximately 245 kg. Its density can be estimated to be equal to 24.0 kN/m$^3$. Dry

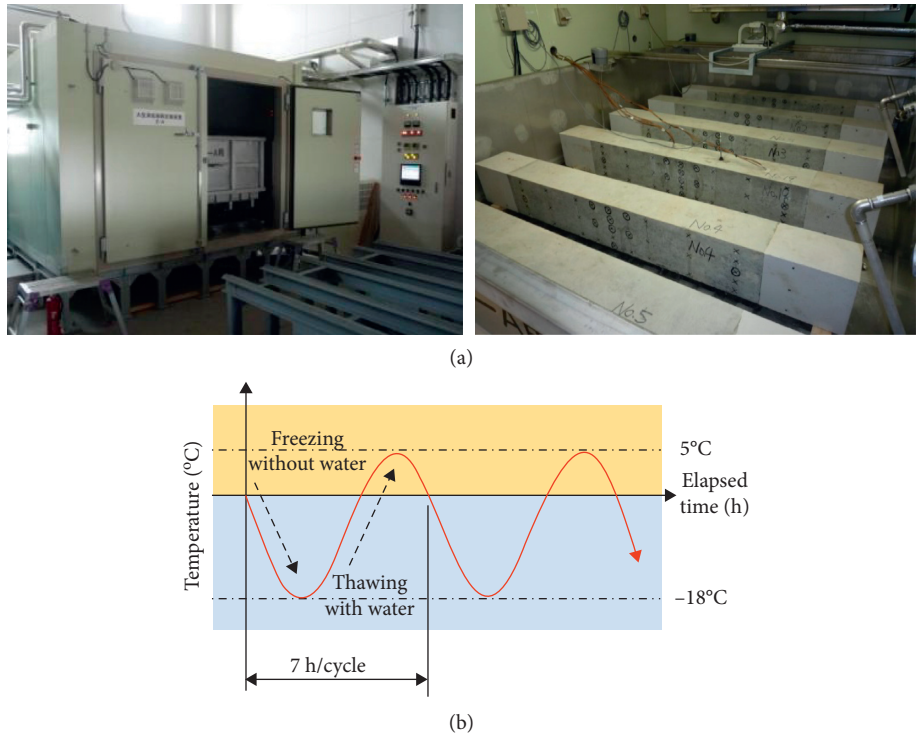


Figure 4: Accelerated deterioration owing to freezing and thawing. (a) Large freeze-thaw test equipment. (b) Freezing and thawing cycles.

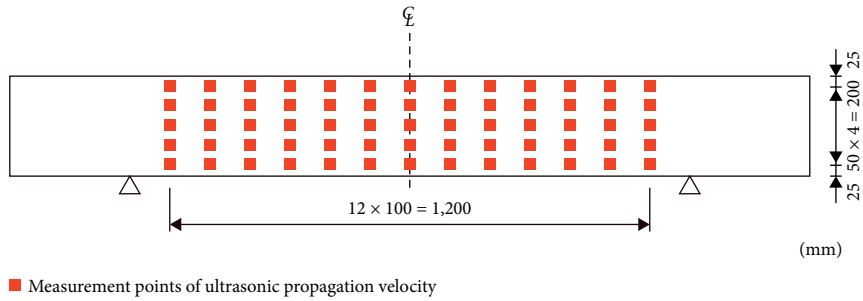


Figure 5: Measuring positions for ultrasonic propagation velocity.

Table 3: List of specimens.

| Specimen | Frost damage | Freezing-thawing cycle (cycle) | Weight falling height $H$ (m) | Measured impact velocity $V$ (m/s) | Input energy $E_k$ (kJ) |
|---|---|---|---|---|---|
| N-H0.5 | Without damage | — | 0.5 | 3.18 | 1.52 |
| N-H1.0 | | | 1.0 | 4.51 | 3.05 |
| D-H0.5 | With damage | 872 | 0.5 | 3.15 | 1.49 |
| D-H1.0-1 | | | 1.0 | 4.51 | 3.05 |
| D-H1.0-2 | | | 1.0 | 4.44 | 2.96 |

masses of D-beams are smaller than those of N-beams. Specifically, in the case of D-H1.0-1, the mass of the beam is the smallest because the edge of the beam is significantly exfoliated. The magnitude relation of the wet mass is almost the same as that of dry mass.

The water absorption ratio $R_a$ of N-beams was approximately equal to 0.6%. This value is much smaller than the typical moisture content of concrete (approximately 3%) [26]. This is because the absorption ratio in this study was evaluated by the total mass of the RC beam, as shown in equation (1). Therefore, it can be observed that water is absorbed slightly inside the beam. The absorption ratios of D-beams are more extensive than those of N-beams. In particular, the absorption ratio of D-H1.0-2 is the largest

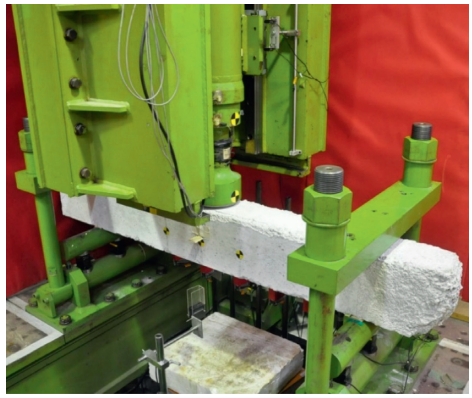

Figure 6: Impact loading test setup.

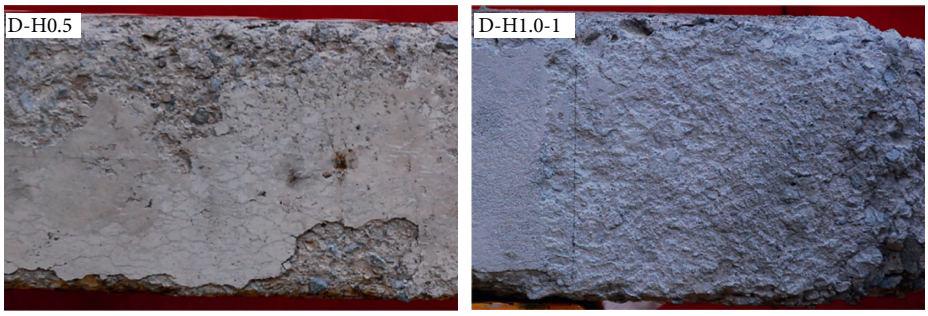


(a)

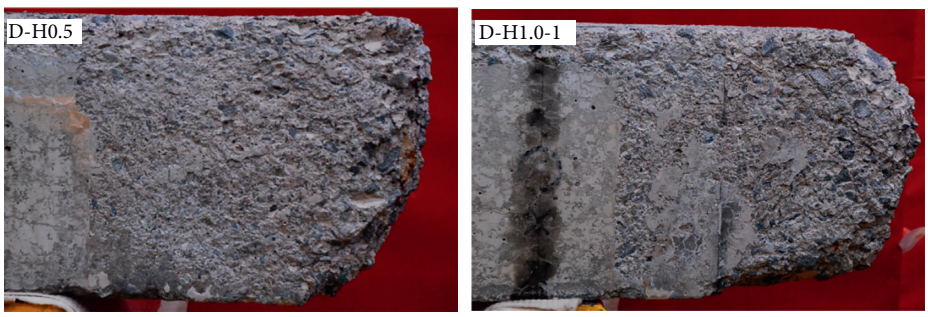


(b)

Figure 7: Deterioration of freezing damage to beams. (a) Upper surface of the beam. (b) Side surface of the beam.

(approximately 2.3%), which is more than four times that of N-beams.

Subsequent measurements of ultrasonic propagation velocity and impact loading experiments were conducted after specimen withdrawal from water and storage in air for approximately five days.

*3.3. Ultrasonic Propagation Velocity Distribution.* Figure 9 shows the measurement results of the ultrasonic propagation velocity. From the figure, the propagation velocity of the N-beam is approximately 4,000 m/s and is equivalent to nondegraded concrete [27]. Conversely, for the D-beam, the propagation velocity in the upper part of the beam is slow. In particular, in the case of the D-H1.0-2 specimen, it can be observed that there is a broad distribution and increased deterioration response for parts that have a low propagation velocity. In the upper part of D-H1.0-2, the ultrasonic propagation velocity is the lowest and is approximately equal to 1,500 m/s. This corresponds to a decrease of 14% in terms of the relative dynamic elastic modulus (RDM) obtained using the following equation [1, 25]:

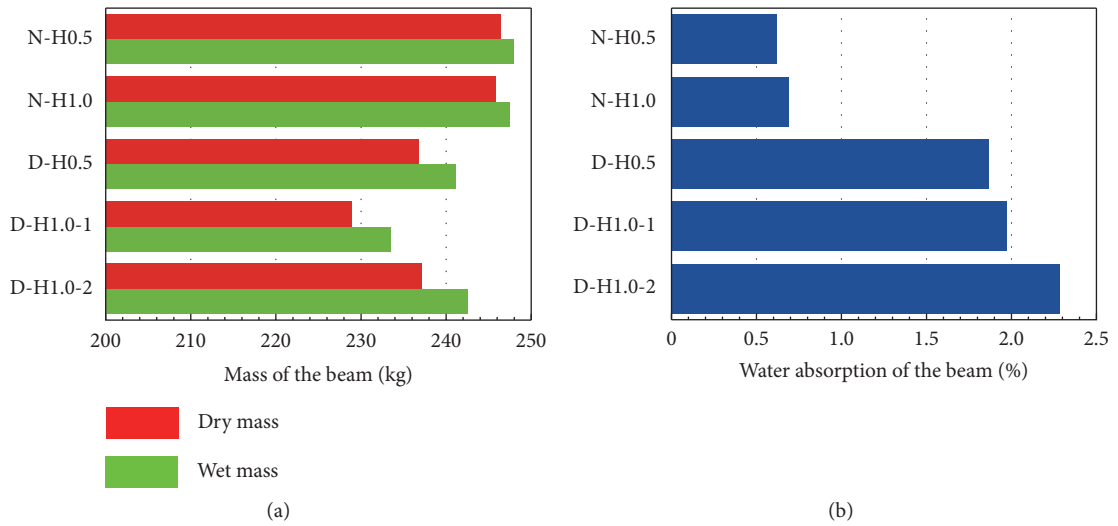


Figure 8: Specimen mass and water absorption. (a) Dry and wet masses and (b) water absorption of the beam.

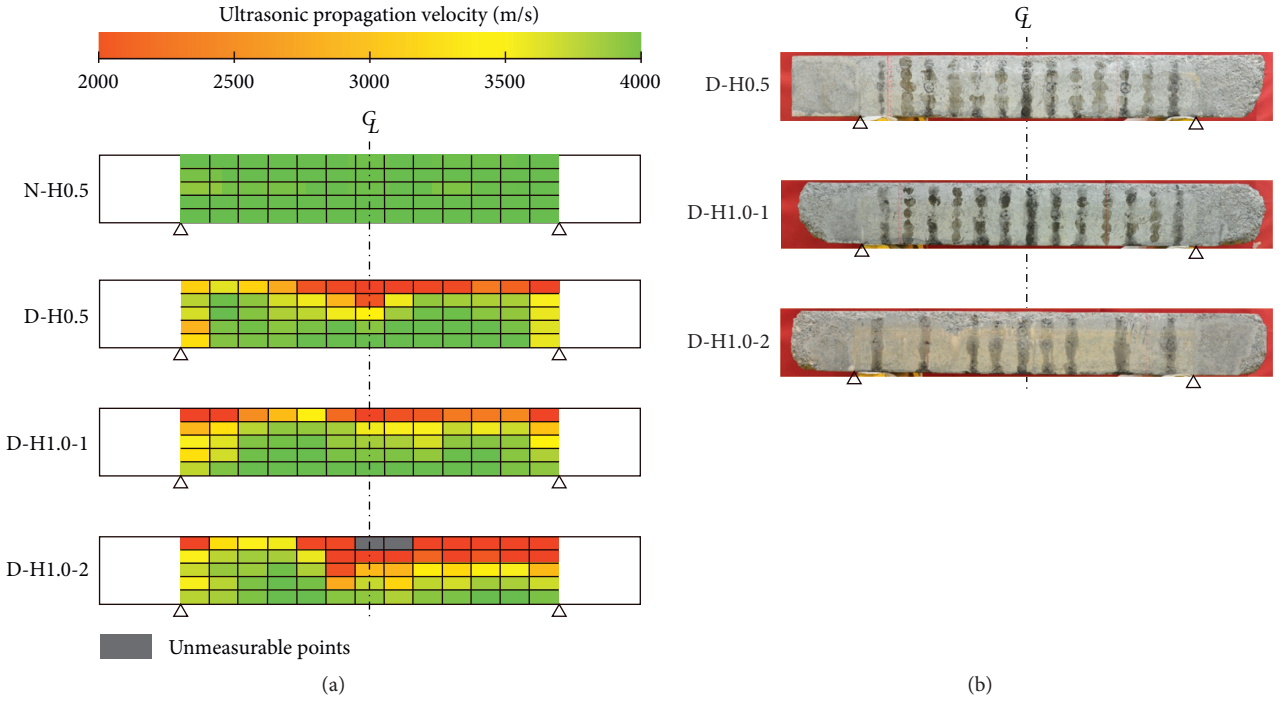


Figure 9: Measured ultrasonic propagation velocity. (a) Distribution of ultrasonic propagation velocity. (b) Condition of RC beam before loading.

$$\mathrm{RDM}(\%) = \frac{v_n^2}{v_0^2} \times 100, \tag{2}$$

where $v_n$ and $v_0$ mean the ultrasonic propagation velocity of concrete at the $n$th cycle and the beginning, respectively.

This indicates that the evaluation of the degree of deterioration based on the propagation velocity of ultrasonic waves corresponds to the evaluation based on the water absorption of the beam.

## 4. Impact Loading Test Results and Discussion

*4.1. Various Response Waveforms.* Figure 10 shows the weight impact force, reaction force, and load-point

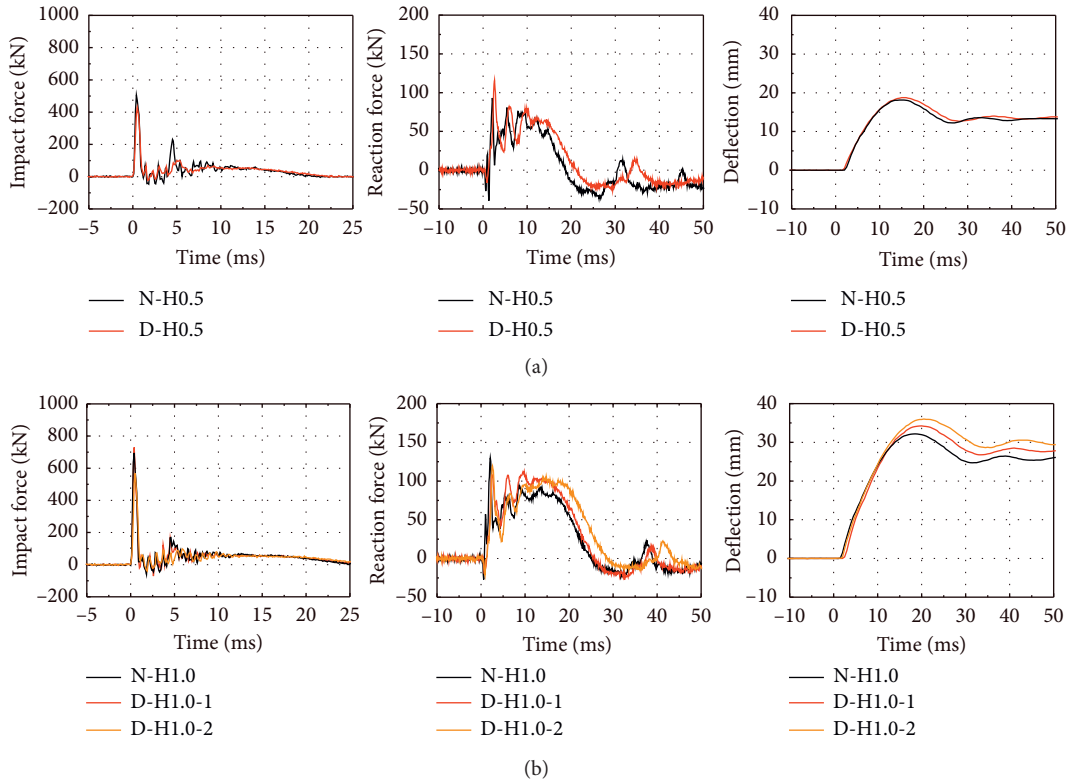


Figure 10: Temporal history response waveforms. (a) $H = 0.5$ m. (b) $H = 1.0$ m.

deflection waveforms of all specimens at each weight falling height $H$. It is observed that the first wave response generated by the weight impact force waveform has duration of approximately 1 ms and amplitudes in the range of 500–700 kN, regardless of the presence or absence of frost damage deterioration. The amplitude tends to increase as the falling height of the weight $H$ increases. Additionally, the maximum impact forces of the D-beams deteriorated by frost damage tend to be smaller than those of the N-beams.

The reaction force waveform shows a waveform characteristic in which the high-frequency component is combined with a half-sine wave. The figure shows that the maximum amplitude and primary wave duration increase as the falling height of the weight increases. The duration can be an indicator of the stiffness of the RC beam when subjected to the same impact loading condition. For $H = 0.5$ m, the duration of the reaction force wave for D-H0.5 is longer than that for N-H0.5. This indicates that the rigidity of D-H0.5 is smaller than that of N-H0.5. For $H = 1.0$ m, the duration of D-H1.0-1 is slightly longer than that of N-H1.0, and that of D-H1.0-2 is approximately 4 ms longer. This tendency corresponds to the degree of deterioration of D-H1.0-2 being greater than D-H1.0-1, as shown in Figure 9(a).

The maximum amplitude of the loading point deflection waveform increases as the set weight falling height $H$ increases. Moreover, for all the specimens, it can be observed that the deflection remains after the first half-sine wave reaches its maximum value. Subsequently, it shifts to a damped free vibration. For $H = 0.5$ m, the maximum deflection is almost the same, regardless of the presence or absence of deterioration. This is because the degree of frost damage deterioration of D-H0.5 is relatively low, and the input energy is small. However, in the case of the specimen D-H0.5, there is minor deflection restoration at a slower rate than that of N-H0.5.

For $H = 1.0$ m, the deflection increases as the degree of deterioration increases. This is attributed to decreased concrete strength, peeling of the upper concrete, and development of diagonal crack openings, as described in the next section.

*4.2. Cracking Properties.* Figure 11 shows the distribution of cracks and ultrasonic propagation velocity in each specimen. All specimens generally exhibit symmetric bending deformation. As shown in Figure 11(a), when $H = 0.5$ m, bending cracks are observed at the center of the beam in both specimens. However, in the case of D-H0.5 with frost damage deterioration, horizontal cracks are observed in the upper side of the beam. The occurrence of horizontal cracks is observed because the upper degradation is significant, as shown by the ultrasonic propagation velocity distribution. In the experiment, high-speed camera images confirmed that split cracking occurred at the interface between the standard part and the deteriorated part during restoration. However, these cracks did not significantly affect the maximum deflection of D-H0.5, as shown in Figure 10(a).

Figure 11(b) shows that when $H = 1.0$ m, bending and diagonal cracks occur regardless of deterioration. In N-H1.0,

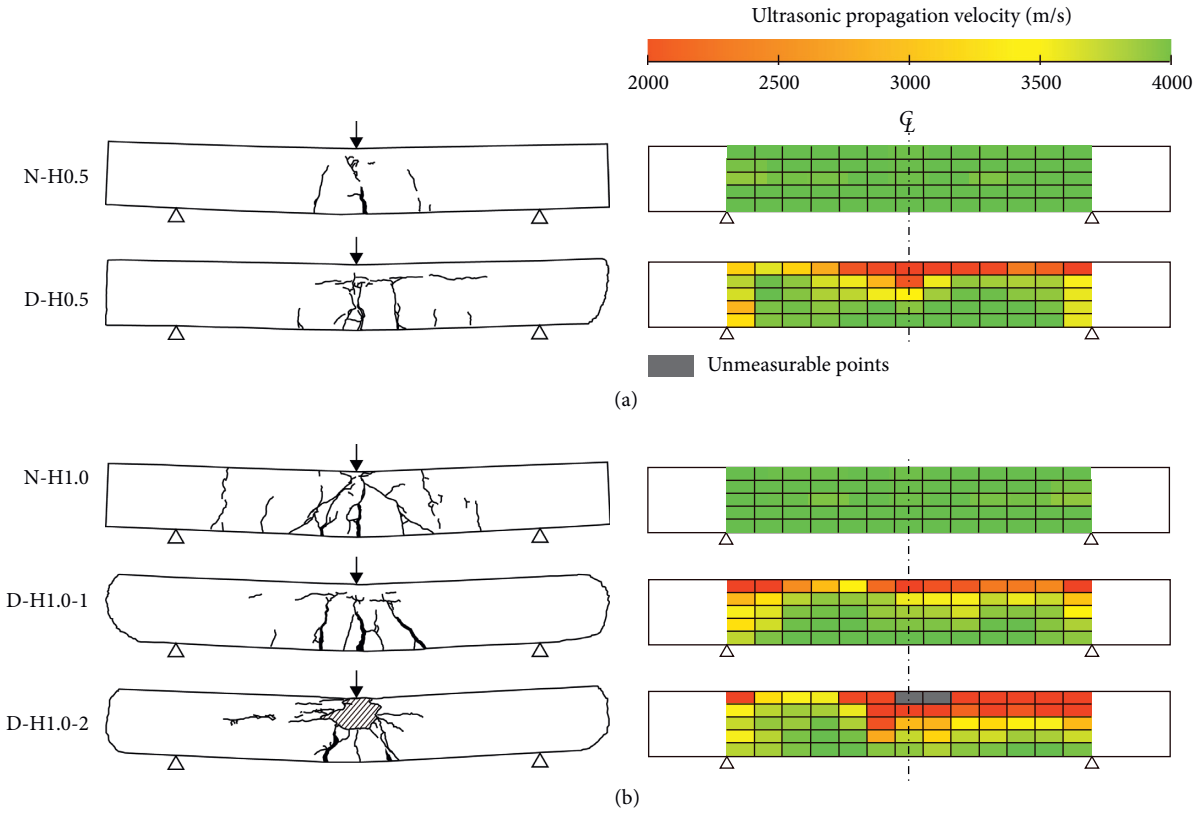


Figure 11: Distribution of cracks and ultrasonic propagation velocity maps. (a) $H = 0.5$ m. (b) $H = 1.0$ m.

cracks occur diagonally in the downward direction at both sides from the loading point, and bending cracks are extensively distributed. Conversely, for beams D-H1.0-1/2, the damage is primarily at the center of both specimens. The damage is localized because a decrease in concrete strength became apparent at the center of the span, wherein a sizeable bending moment and shear force were applied. The cover concrete around the mid-span of the specimen D-H1.0-2, which has a high degree of deterioration, was peeled off. These properties correspond to the ultrasonic velocity distribution. It is probable that, owing to these damages, the maximum deflection of D-H1.0-2 was more extensive than that of N-H1.0, as shown in Figure 10(b).

Figure 12 shows the cracking behavior of the upper edge concrete at the center of the span after the experiment when the falling height $H = 1.0$ m. From the figure, the exfoliation of the cover concrete occurred at the weight collision part in each specimen. In the case of the nondegraded N-H1.0, delamination occurred along the beam width direction area. In contrast, in the degraded D-H1.0-1/2, the upper surface of the beam was peeled off. A peeled region is also observed in the axial direction. This tendency is remarkable in the D-H1.0-2, where the response deflection was large.

Figure 13 shows high-speed camera images of the progress of cracking at a falling height $H = 1.0$ m. Results show that in the case of the N-H1.0 without deterioration, bending and diagonal cracks occurred at the elapsed time $t = 2.5$ ms. The initial bending rigidity of N-H1.0 was higher than other deteriorated beams, so that diagonal cracks such as punching shear cracks occurred. At $t = 5$ ms, in addition to the bending cracks at the center of the span, bending shear cracks at both ends were observed, and these cracks were opened at $t = 10$ ms. At $t = 20$ ms, the width of the cracks became more extensive, with concrete compressive failure at the upper edge.

In the cases of the deteriorated D-H1.0-1, there are no diagonal cracks at the elapsed time $t = 2.5$ ms. This is due to the appearance of increased damage at the weight collision part (Figure 12). Subsequently, in the case of the D-H1.0-1, a bending crack opened at $t = 5$ ms, and a diagonal crack occurred on the right side at $t = 10$ ms. A bending crack appeared on the left side. At $t = 20$ ms, the diagonal crack on the right side opened further. This result is probably attributed to the fact that the degree of deterioration on the right side was slightly large. As shown in Figure 10(b), the effect of these cracks on the maximum deflection of the RC beam was not so large.

In the case of D-H1.0-2, three bending cracks occurred at $t = 5$ ms. These cracks opened at $t = 10$ and 20 ms. The crack on the left side had an unusually large opening that corresponds to the ultrasonic propagation velocity distribution, wherein the damage was concentrated on the highly degraded part. It is considered that the maximum deflection of D-H1.0-2 increased owing to the occurrence of these multiple bending crack openings.

Therefore, it became clear that in the case of RC beams deteriorated owing to frost damage, the damage tends to concentrate on the highly deteriorated parts. It is possible to evaluate the impact resistance of RC beams that have been

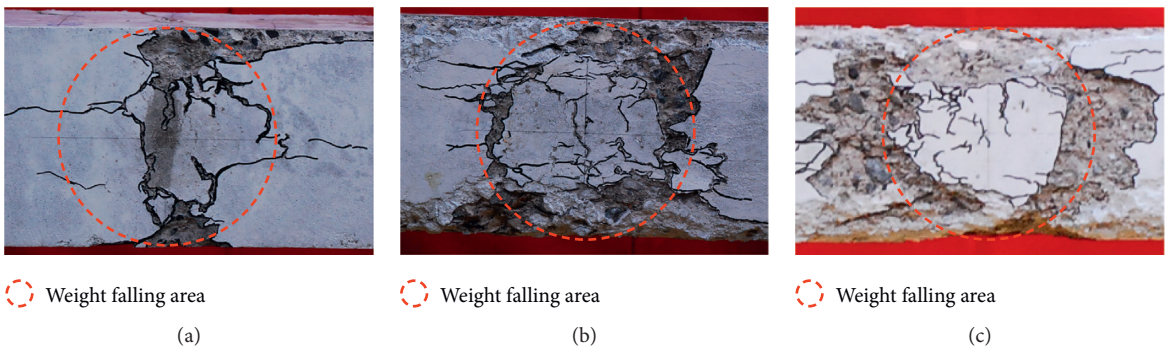


Figure 12: Cracking behavior of the upper edge concrete at the mid-span. (a) N-H1.0. (b) D-H1.0-1. (c) D-H1.0-2.

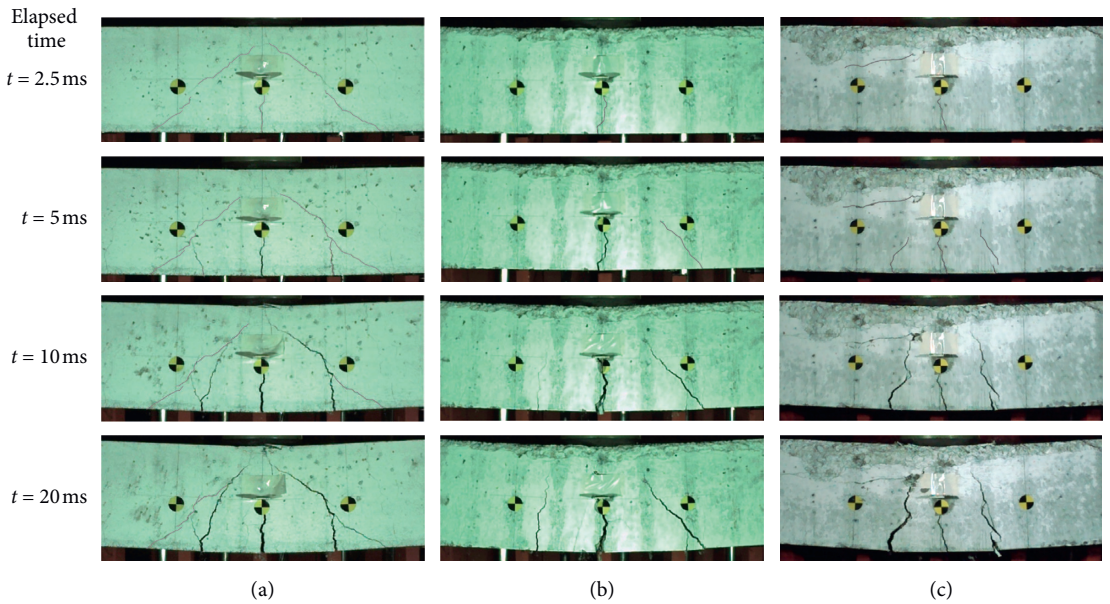


Figure 13: Crack growth at the falling height $H = 1.0$ m. (a) N-H1.0. (b) D-H1.0-1. (c) D-H1.0-2.

degraded by frost damage based on the ultrasonic propagation velocity distribution.

*4.3. Relationship between Residual Deflection and Input Energy.* Figure 14 shows the relationship between the residual deflection and input energy. The figure also shows the relational expression between the input energy $E_k$ and the residual deflection $\delta_{rs}$ evaluated using equation (3) [28]. This equation can estimate the residual deflection $\delta_{rs}$ by estimating the input energy $E_k$ owing to the falling of the weight and the calculated bending strength $P_{us}$ of the RC beam.

$$\delta_{rs} = 0.42\frac{E_k}{P_{us}}. \quad (3)$$

Herein, $E_k$ is the input energy (kJ), and $P_{us}$ is the static bending capacity (kN) of the beam. The static bending capacity $P_{us}$ (56.8 kN) of the beam was calculated according to the JSCE concrete specifications [23] using the material properties of concrete and rebar without degradation. For the N-beams without deterioration, the residual deflection

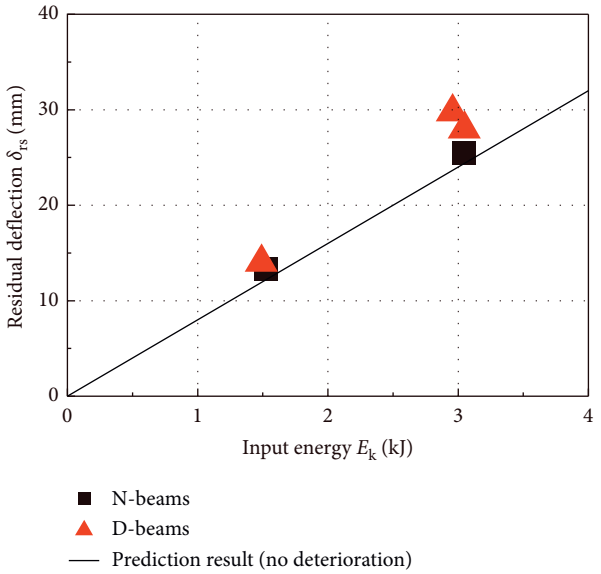


Figure 14: Relationship between residual deflection and input energy.

proportionally increased as a function of the input energy similar to equation (3). Conversely, the residual deflections of the D-beams are larger than those of the N-beams. In particular, the residual deflection of D-H1.0-2 is approximately 1.2 times larger than that of N-H1.0. This may be due to the microcracks and scaling caused by frost damage and the decrease in the bending capacity of the RC beam due to decreased compressive strength.

Therefore, it is observed that when the ultrasonic propagation velocity of the upper cover concrete is approximately 1,500 m/s (14% relative dynamic elastic modulus), the residual deflection $\delta_{rs}$ of the RC beam is increased by approximately 20%. Additionally, according to the existing residual deflection calculation formula (equation (3)), an increase of 20% in the residual deflection $\delta_{rs}$ corresponds to a decrease of approximately 17% in the bending capacity of the RC beam $P_{us}$.

## 5. Conclusions

In this study, RC beams with shear reinforcement were fabricated, and weight falling impact tests were performed to investigate the impact resistance behavior of RC beams with frost damage deterioration. The RC beams suffered frost damage induced by successive freezing and thawing tests. The surface was scaled considerably, and the coarse aggregate was exposed. The degree of deterioration was evaluated by the rate of change of the ultrasonic propagation velocity. As a result, the following conclusions were inferred.

(1) The ultrasonic propagation velocity of RC beams was reduced considerably by the freeze–thaw action of approximately 900 cycles. At the upper edge of the RC beam, the ultrasonic wave propagation velocity decreased from 4,000 m/s to 1,500 m/s in some parts. This corresponds to a relative dynamic elastic modulus of approximately 14%. At this time, the water absorption ratio of the RC beam was approximately 2.3%.

(2) In the case of RC beams without deterioration, diagonal cracks extended downward from the loading point to both sides, and bending cracks were extensively distributed owing to the impact loading. Conversely, in the case of RC beams with frost damage, the damage was concentrated near the loading point. The concrete on the upper edge was peeled off, and multiple bending cracks were generated.

(3) The residual deflection of RC beams with frost damage increased up to 20% compared with beams without frost damage. The increase in residual deflection was primarily related to the peeling of concrete at the collision site and the opening of multiple bending cracks.

(4) According to the existing residual deflection calculation formula, an increase of 20% in the residual deflection corresponds to a decrease of approximately 17% in the bending capacity of the RC beam.

In the future, we will investigate the actual compressive strength and frost damage depth of concrete after frost damage deterioration of the RC beams. The bending strength would be calculated based on survey results, and the impact resistance would then be evaluated.

## Data Availability

All the data used to support the findings of this study are available from the corresponding author upon request.

## Conflicts of Interest

The authors declare that they have no conflicts of interest regarding the publication of this paper.

## Acknowledgments

For deflection measurement, the authors used a high-speed camera owned by the Civil Engineering Research Institute for Cold Regions. The authors would like to thank Editage (http://www.editage.com) for English language editing. This study was supported by the Foundation of JSPS KAKENHI (Grant no. 19H02394).

## References

[1] K. Z. Hanjari, P. Utgenannt, and K. Lundgren, "Experimental study of the material and bond properties of frost-damaged concrete," *Cement and Concrete Research*, vol. 41, no. 3, pp. 244–254, 2011.

[2] M. Hasan, H. Okuyama, Y. Sato, and T. Ueda, "Stress-strain model of concrete damaged by freezing and thawing cycles," *Journal of Advanced Concrete Technology*, vol. 2, no. 1, pp. 89–99, 2004.

[3] L. Qin, Y. Song, H. Chen et al., "Mechanical property and failure criterion of concrete under biaxial tension and compression after freeze-thaw cycling," *Chinese Journal of Rock Mechanics and Engineering*, vol. 24, no. 5, pp. 1740–1745, 2005.

[4] H. S. Shang and Y. P. Song, "Experimental study of strength and deformation of plain concrete under biaxial compression after freezing and thawing cycles," *Cement and Concrete Research*, vol. 36, no. 10, pp. 1857–1864, 2006.

[5] M. Hasan, T. Ueda, and Y. Sato, "Stress-strain relationship of frost-damaged concrete subjected to fatigue loading," *Journal of Materials in Civil Engineering*, vol. 20, no. 1, pp. 37–45, 2008.

[6] C. Zou, J. Zhao, F. Liang et al., "Degradation of mechanical properties of concrete caused by freeze-thaw action," *Journal of Building Engineering*, vol. 29, no. 1, pp. 117–123, 2008.

[7] A. Duan, W. Jin, and J. Qian, "Effect of freeze-thaw cycles on the stress-strain curves of unconfined and confined concrete," *Materials and Structures*, vol. 44, no. 7, pp. 1309–1324, 2011.

[8] L. Petersen, L. Lohaus, and M. A. Polak, "Influence of freezing-and-thawing damage on behavior of reinforced concrete elements," *Journal of ACI Materials*, vol. 104, no. 4, pp. 369–378, 2007.

[9] J. M. L. Reis and A. J. M. Ferreira, "Freeze-thaw and thermal degradation influence on the fracture properties of carbon and glass fiber reinforced polymer concrete," *Construction and Building Materials*, vol. 20, no. 10, pp. 888–892, 2006.

[10] T. S. Shih, G. C. Lee, and K. C. Chang, "Effect of freezing cycles on bond strength of concrete," *Journal of Structural Engineering*, vol. 114, no. 3, pp. 717–726, 1988.

[11] G. Fagerlund, M. Janz, and B. Johannesson, *Effect of Frost Damage on the Bond between Reinforcement and Concrete, Report*, Division of Building Materials, Lund Institute of Technology, Lund, Sweden, 1994.

[12] X. Ji, Y. Song, and Y. Liu, "Effect of freeze-thaw cycles on bond strength between steel bars and concrete," *Journal of Wuhan University of Technology-Materials and Science Ed.*vol. 23, no. 4, pp. 584–588, 2008.

[13] M. Hassanzadeh and G. Fagerlund, "Residual strength of the frost-damaged reinforced concrete beams," in *Proceedings of the III European Conference on Computational Mechanics*, p. 366, Springer, Newport, RI, USA, January 2006.

[14] A. Duan, Z. Li, W. Zhang et al., "Flexural behaviour of reinforced concrete beams under freeze–thaw cycles and sustained load," *Structure and Infrastructure Engineering*, vol. 13, pp. 1–9, 2016.

[15] D. F. Cao, X. C. Qin, S. P. Meng et al., "Evaluation of prestress losses in prestressed concrete specimens subjected to freeze–thaw cycles," *Structure and Infrastructure Engineering*, vol. 12, no. 2, pp. 1–12, 2015.

[16] D. F. Cao, Z. Ma, W. Ge et al., "Experimental study on the eccentric compressive behaviors of RC columns after freeze–thaw cycles," *Journal of Southeast University (Natural Science Edition)*, vol. 44, no. 1, pp. 38–45, 2014.

[17] D. F. Cao, K. F. Zhou, M. Zhou, W. J. Ge, and B. Y. Wang, "Study on the shear behaviors of RC beams after freeze-thaw cycles," *Applied Mechanics and Materials*, vol. 488-489, pp. 750–754, 2014.

[18] S. Xu, A. Li, Z. Ji, and Y. Wang, "Seismic performance of reinforced concrete columns after freeze-thaw cycles," *Construction and Building Materials*, vol. 102, pp. 861–871, 2016.

[19] K. Z. Hanjari, P. Kettil, and K. Lundgren, "Modelling the structural behaviour of frost-damaged reinforced concrete structures," *Structure and Infrastructure Engineering*, vol. 9, no. 5, pp. 416–431, 2013.

[20] A. Li, "Study on seismic behavior of reinforced concrete column under low cyclic loading after freeze-thaw cycles," M. S. thesis, Xi'an University of Architecture & Technology, Xi'an, China, 2014.

[21] Y. Kurihashi, M. Mizuta, A. Shimata, and N. Kishi, "Impact resistant behavior of RC beam damaged by freeze-thaw action," in *Proceedings of the 8th international conference on concrete under severe conditions-environment & loading*, pp. 745–750, Lecco, Italy, September 2016.

[22] Y. Kurihashi, M. Mizuta, N. Kishi, and K. Ikeda, "Experimental study on impact resistant behavior and residual capacity of RC beam damaged by freezing and thawing," *Journal of Structural Engineering*, vol. 62A, pp. 1053–1060, 2017, in Japanese.

[23] Japan Society of Civil Engineers, "Standard specifications for concrete structures–structural performance verification," *JSCE Guidelines for Concrete*, vol. 3, 2005.

[24] Japanese Industrial Standards, *JIS 1148, Method of test for Resistance of Concrete to Freezing and thawing*, Japanese Industrial Standards, Japan, 2010.

[25] S. Xu, A. Li, and H. Wang, "Bond properties for deformed steel bar in frost-damaged concrete under monotonic and reversed cyclic loading," *Construction and Building Materials*, vol. 148, pp. 344–358, 2017.

[26] B. D. Liu, W. J. Lv, L. Li, and P. F. Li, "Effect of moisture content on static compressive elasticity modulus of concrete," *Construction and Building Materials*, vol. 69, pp. 133–142, 2014.

[27] N. Mita and T. Takigushi, "Principle of ultrasonic tomography for concrete structures and non-destructive inspection of concrete cover for reinforcement," *Pacific Journal of Mathematics for Industry*, vol. 10, p. 6, 2018.

[28] N. Kishi and H. Mikami, "Empirical formulas for designing reinforced concrete beams under impact loading," *ACI Structural Journal*, vol. 109, no. 4, pp. 509–519, 2012.